Continuum models for pantographic blocks with second gradient energies which are incomplete

Maximilian Stilz [a,*], Francesco dell'Isola [b], Ivan Giorgio [b], Victor A. Eremeyev [c,d], Georg Ganzenmüller [a], Stefan Hiermaier [a,e]

[a] *INATECH, Albert-Ludwigs-Universität, Freiburg, Germany*
[b] *Department of Civil, Construction-Architecture and Environmental Engineering, University of L'Aquila, L'Aquila, Italy*
[c] *Department of Mechanics of Materials and Structures, Faculty of Civil and Environmental Engineering, Gdańsk University of Technology, Gdańsk, Poland*
[d] *DICAAR, Universitá degli Studi di Cagliari, Cagliari, Italy*
[e] *Fraunhofer Institute for High-Speed Dynamics, Ernst-Mach Institut, EMI, Freiburg, Germany*

ARTICLE INFO

Keywords:
Generalized continuum mechanics
Second gradient materials
Metamaterials

ABSTRACT

We postulate a deformation energy for describing the mechanical behavior of so called pantographic blocks, that is bodies constituted by stacking of N layers of pantographic sheets. We remark that the pantographic effect is limited in the plane of pantographic sheets and therefore only the second derivatives of transverse displacements along the pantographic fibers appear in the chosen deformation energy. We use this novel energy to predict the behavior of pantographic blocks when subjected to : (i) compression and traction test, (ii) torsion, (iii) shear and (iv) bending. A linearization of the energy shows one floppy mode in addition to the rigid body motions, assuming perfect pivots, similar to pantographic sheets.

1. Introduction

Pantographic sheets are a class of 2D continua which call for models based on more generalized theories of continuum mechanics for a predictive description of their deformation [1–6]. Theories involving the second gradient of displacement in the energy [7–10] have been shown to successfully fulfill these needs by comparing experiments and simulations [11–14]. In reality, the 3D printed objects are not homogeneous in their surface normal direction as often assumed in plate theory, but rather they are chiral with an offset between the two layers of fibers. The offset has been addressed in some studies specifically [15–17]. Some experiments, like the three-point-bending test, are challenging to perform on a thin sheet as buckling phenomena complicate the process. For this purpose a pantographic block has been designed as layers of pantographic sheets [18]. So far only the in-plane behavior was modeled which matches the one of the sheet. For future research we find it important to include the influence of the pivots with some basic kinematic assumptions in their elongation, shear and twist. We utilize the continuum model for pantographic sheets in three-dimensional space from Giorgio et al. [19] and embed it in a three-dimensional continuum with the coupling in the third direction by the aforementioned pivot kinematics. The resulting continuum model retains the second gradient specifics for the planes of pantographic sheets and adds only first gradient components in the additional dimension.

In future research, the validation of our model in experiments will rely on novel techniques in 3D imaging such as Digital Volume Correlation [20]. Dynamic [21] and damage phenomena [14,17,22,23] which have been studied for other pantographic structures are also a topic for future research and will be not covered in this work.

In the following we employ covariant (subscript) and contravariant (superscript) index notation with summation over repeated indices.

2. Geometry

A pantographic sheet as depicted in Fig. 1(top) consists of two families of fibers each in a parallel plane with usually a 90°-angle between the fibers in the reference configuration. A pivot along the normal of the planes connects fibers from each plane with the lengths of the pivot being at least the offset length h_p between these planes. We can now imagine adding additional parallel planes with the same offset and alternating fiber orientation so that they can be connected along the further extended pivots. The resulting structure consists of $2N$ layers of the fiber planes (or N layers of pantographic sheets) with $N \in \frac{1}{2}\mathbb{N}$ interconnected by pivots with total length $(2N-1)h_p$ depicted in Fig. 1(bottom).

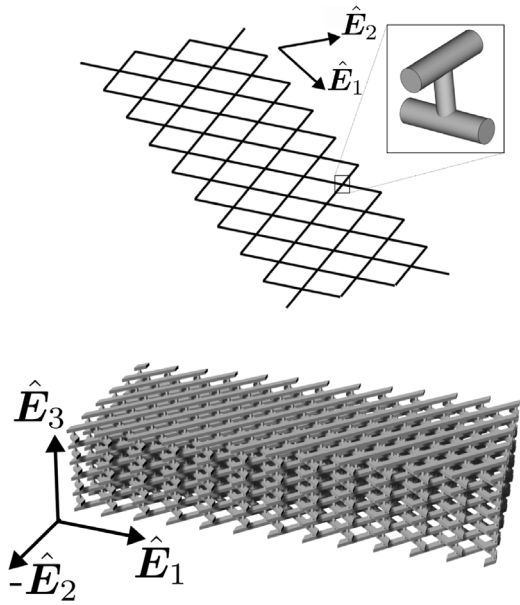*E-mail address:* maximilian.stilz@inatech.uni-freiburg.de (M. Stilz).

Fig. 1. (Top): The fiber lattice basis of the pantographic sheet with enhanced detail of a junction. (Bottom): A CAD image of a pantographic block with 5.5 layers of pantographic sheets or 11 layers of pantographic planes.

3. Deformation energy

It is necessary to postulate a class of deformation energies in order to design appropriately the experimental tests that we have to perform in order to understand the exotic behavior of pantographic blocks. The postulation was inspired by the following concept: in the plane of pantographic sheets the energy stored in deformation phenomena is exactly that postulated for pantographic sheets in 3D motion [19], but calculating its volume density considering the number of pantographic sheets interconnected per unit line. For the remaining (nonlinear) deformation measures needed to complete a 3D description, we assume that the corresponding deformation energy is simply quadratic.

For better understanding, we recapitulate the energy of pantographic sheets [19].

3.1. Lattice plate kinematics

The reference configuration κ could be represented as a plane area $\Omega \subset \mathbb{R}^2$ with a position vector $\mathbf{X}$ and with two families of lines which model the embedded fibers of a pantographic sheet. We define the unit tangent vectors of each family to be $\boldsymbol{D}^{(\alpha)}$, $\alpha \in \{1, 2\}$. Additionally, we define $\boldsymbol{N} = \boldsymbol{D}^{(1)} \times \boldsymbol{D}^{(2)}$ as the fibers' normal and $\boldsymbol{M}^{(\alpha)} = \boldsymbol{D}^{(\alpha)} \times \boldsymbol{N}$ as the completion of the fibers' triad. Here $\times$ is the cross product. Further we call $\chi : \kappa \mapsto \chi$ an invertible mapping from the reference κ into the current χ placement, so $x = \chi(X)$, where $\boldsymbol{x} = x^i \hat{\boldsymbol{e}}_i$ is a position vector in χ with Cartesian basis $\hat{\boldsymbol{e}}_i$ and $\boldsymbol{X} = X^A \hat{\boldsymbol{E}}_A$ in κ with Cartesian basis $\hat{\boldsymbol{E}}_A$ (see Fig. 2 left).

The tangent vectors $\boldsymbol{d}^{(\alpha)}$ of the embedded fibers then become the directional derivative of $\boldsymbol{x}$ on the surface in direction $\boldsymbol{D}^{(\alpha)}$ and therefore are calculated through

$$\boldsymbol{d}^{(\alpha)} = D\chi(\boldsymbol{X})[\boldsymbol{D}^{(\alpha)}] = \frac{\partial \chi(\boldsymbol{X})}{\partial \boldsymbol{X}} \boldsymbol{D}^{(\alpha)} \tag{1}$$

$$= \boldsymbol{F} \boldsymbol{D}^{(\alpha)} = F_A^i \left(D^{(\alpha)}\right)^A \hat{\boldsymbol{e}}_i , \tag{2}$$

and we define the unit tangent vector as

$$\boldsymbol{e}^{(\alpha)} = \frac{\boldsymbol{d}^{(\alpha)}}{\|\boldsymbol{d}^{(\alpha)}\|} = \frac{\boldsymbol{d}^{(\alpha)}}{\rho} , \tag{3}$$

where $\boldsymbol{F}$ denotes the deformation gradient of the mapping χ and $\rho^{(\alpha)} = \|\boldsymbol{d}^{(\alpha)}\|$ the stretch of the fiber. In each point we find the unit normal of the (smooth) surface with the two tangent vectors

$$\boldsymbol{n} = \frac{\boldsymbol{e}^{(1)} \times \boldsymbol{e}^{(2)}}{\|\boldsymbol{e}^{(1)} \times \boldsymbol{e}^{(2)}\|} , \tag{4}$$

and apply the kinematic constraint, that this is also the normal of the fibers serving as an orientation for their cross-section. To complete the beam triad we add their bitangent vector

$$\boldsymbol{m}^{(\alpha)} = \boldsymbol{n} \times \boldsymbol{e}^{(\alpha)} \tag{5}$$

(see Fig. 2 right).

3.2. Fiber and surface deformation measures

Based on these definitions we can propose deformation measures of the fibers based on properties of the surface deformation. The change in lengths is measured with

$$\varepsilon^{(\alpha)} = \|\boldsymbol{d}^{(\alpha)}\| - 1 . \tag{6}$$

With the derivative in the corresponding fiber direction $\boldsymbol{e}_{,\alpha}^{(\alpha)} = \frac{\partial [e^{(\alpha)}]^i}{\partial X^A} \left[D^{(\alpha)}\right]^A \hat{\boldsymbol{e}}_i = \left[e^{(\alpha)}\right]^i_{,A} \left[D^{(\alpha)}\right]^A \hat{\boldsymbol{e}}_i$ we define, based on the deformation of a curve, the curvature measures separated in in-plane or normal curvature, out-of-plane curvature and torsion

$$\kappa_n^{(\alpha)} = -\boldsymbol{m}^{(\alpha)} \cdot \boldsymbol{e}_{,\alpha}^{(\alpha)}, \tag{7}$$

$$\kappa_g^{(\alpha)} = \boldsymbol{n} \cdot \boldsymbol{e}_{,\alpha}^{(\alpha)}, \tag{8}$$

$$\tau^{(\alpha)} = \boldsymbol{e}^{(\alpha)} \cdot \boldsymbol{m}_{,A}^{(\alpha)}. \tag{9}$$

Additionally we define the shearing deformation measure $\gamma^{(12)}$ between the fiber families

$$\sin \gamma^{(12)} = \boldsymbol{e}^{(1)} \cdot \boldsymbol{e}^{(2)} . \tag{10}$$

3.3. Lattice block kinematics

In the reference placement a lattice block of thickness H takes a volume $\Pi \subset \mathbb{R}^3$, $\Pi = \Omega \times [0, H]$ Just as the fibers were embedded in Ω, they are embedded in Π. To describe the kinematics in the additional dimension we introduce pivot fibers with their tangent vector in the reference configuration $\boldsymbol{D}^{(3)} = \boldsymbol{D}^{(1)} \times \boldsymbol{D}^{(2)} = \boldsymbol{N}$ and $\boldsymbol{d}^{(3)} = \boldsymbol{F} \boldsymbol{D}^{(3)} = \|\boldsymbol{d}^{(3)}\| \boldsymbol{e}^{(3)}$.

3.4. Pivot deformation measures

Just as for the fibers we define the pivot's stretch as

$$\varepsilon^{(3)} = \rho^{(3)} - 1 = \|\boldsymbol{d}^{(3)}\| - 1 . \tag{11}$$

The shear of the pivot in each fiber direction is measured with the angles $\gamma^{(31)}$ and $\gamma^{(32)}$

$$\sin \gamma^{(31)} = \boldsymbol{e}^{(3)} \cdot \boldsymbol{e}^{(1)}, \qquad \sin \gamma^{(32)} = \boldsymbol{e}^{(3)} \cdot \boldsymbol{e}^{(2)} . \tag{12}$$

We can approximate the twist of the pivot by Eq. (10).

3.5. Energy density

With these deformation measures we postulate the energy density to be quadratic in these measures. Firstly, the fiber contribution becomes

$$w_f = \sum_\alpha \frac{1}{2} K_e \left(\varepsilon^{(\alpha)}\right)^2 + \frac{1}{2} K_n \left(\kappa_n^{(\alpha)}\right)^2 + \frac{1}{2} K_g \left(\kappa_g^{(\alpha)}\right)^2$$
$$+ \frac{1}{2} K_t \left(\tau^{(\alpha)}\right)^2 + \frac{1}{2} K_s^{(12)} \left(\gamma^{(12)}\right)^2 \tag{13}$$

and the pivot contributions are

$$w_p = \frac{1}{2} K_e^{(3)} \left(\varepsilon^{(3)}\right)^2 + \frac{1}{2} K_s^{(31)} \left(\gamma^{(31)}\right)^2 + \frac{1}{2} K_s^{(32)} \left(\gamma^{(32)}\right)^2$$
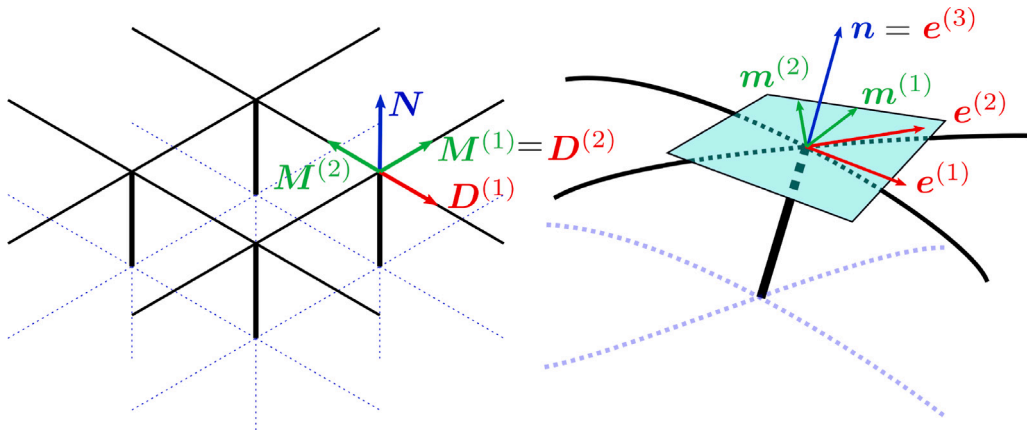
Fig. 2. Embedded lattice structure in the reference configuration and a detail of the actual configuration with kinematic descriptors.
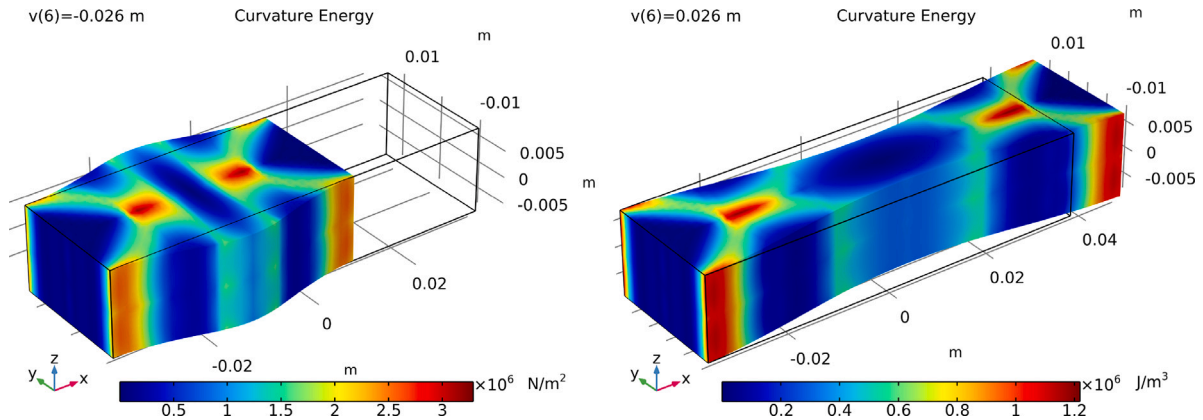

Fig. 3. Compression and traction test by displacement boundary conditions. The colors indicate the amount of deformation energy density by curvature of the embedded fibers. (For interpretation of the references to color in this figure legend, the reader is referred to the web version of this article.)
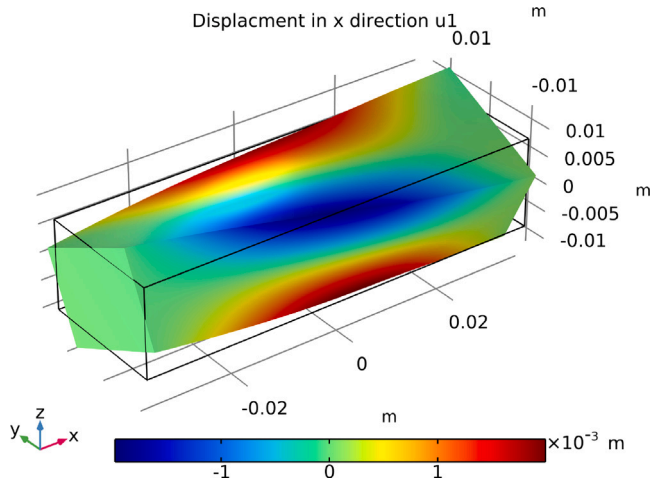
Fig. 4. Torsion test by displacement boundary conditions. The colors indicate the displacement in x direction. (For interpretation of the references to color in this figure legend, the reader is referred to the web version of this article.)

$$+ K_c \left[\varepsilon^{(3)} \left(\varepsilon^{(1)} + \varepsilon^{(2)} \right) \right] . \tag{14}$$

The last term is introduced as a correction term to account for a Poisson effect by coupling the elongation of the fibers with the pivot's. K_e, K_n, K_g, K_t, $K_s^{(12)}$, $K_e^{(3)}$, $K_s^{(31)}$, $K_s^{(32)}$ and K_c are stiffness coefficients based on material and geometry parameters of the fibers and pivots, also accounting for the density of beams and pivots in the corresponding discrete structure.

4. Reference configuration

For the following analysis we choose the reference configuration with

$$\boldsymbol{D}^{(1)} = \frac{1}{\sqrt{2}} \left(\hat{\boldsymbol{E}}_1 + \hat{\boldsymbol{E}}_2 \right) = \frac{1}{\sqrt{2}} (1, 1, 0)^\top , \tag{15}$$

$$\boldsymbol{D}^{(2)} = \frac{1}{\sqrt{2}} \left(\hat{\boldsymbol{E}}_2 - \hat{\boldsymbol{E}}_1 \right) = \frac{1}{\sqrt{2}} (-1, 1, 0)^\top , \tag{16}$$

$$\boldsymbol{D}^{(3)} = \hat{\boldsymbol{E}}_3 = (0, 0, 1)^\top \tag{17}$$

5. Linearization and floppy modes

To determine the system's floppy modes, meaning deformation modes with zero energy, we conduct a linearization of the model using the approach from [24,25] with the expansion for small deformations

$$\chi(\boldsymbol{X}) = \boldsymbol{X} + \eta \boldsymbol{u}(\boldsymbol{X}) \tag{18}$$

$$\boldsymbol{H} := \nabla \boldsymbol{u} \tag{19}$$

$$\boldsymbol{F} = \mathbb{I} + \eta \boldsymbol{H} \tag{20}$$

$$\nabla \boldsymbol{F} = F_{A,B}^i = \eta \nabla \boldsymbol{H} = \eta H_{A,B}^i \tag{21}$$

This leads for the deformation measures in first order of η to

$$\varepsilon^{(\alpha)} \approx \eta \boldsymbol{H} \boldsymbol{D}^{(\alpha)} \cdot \boldsymbol{D}^{(\alpha)} = \eta H_A^i \left[D^{(\alpha)} \right]^A D_i^{(\alpha)} \tag{22}$$
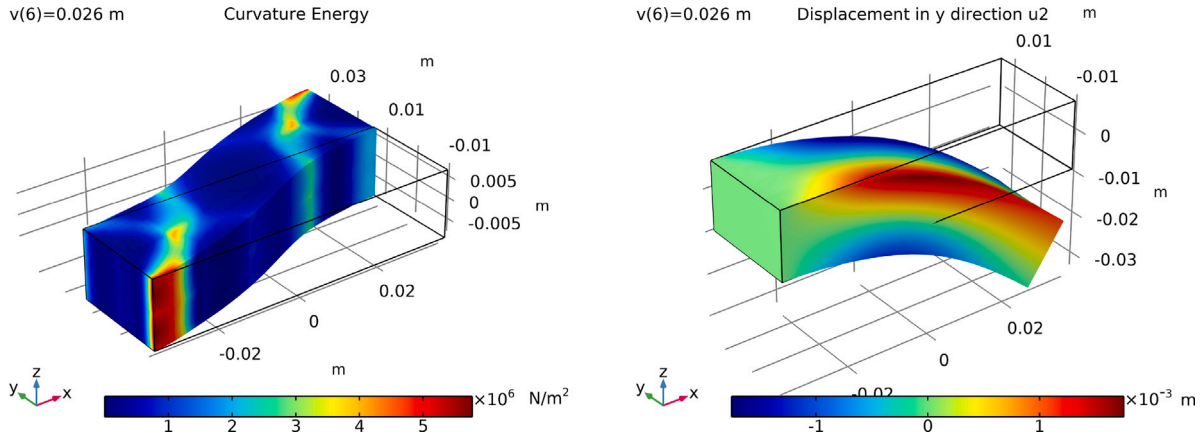
Fig. 5. The shear test on the left is imposed by displacement boundary conditions with colors indicating the amount of deformation energy density by curvature of the embedded fibers. The bending test on the right was conducted with a surface force dead load in z direction. The colors indicate the displacement in y direction, showing the in-plane deformation of the pantographic sheets. (For interpretation of the references to color in this figure legend, the reader is referred to the web version of this article.)

$$\kappa_g^{(\alpha)} \approx \eta \mathbf{N} \nabla \mathbf{H} : \mathbf{D}^{(\alpha)} \otimes \mathbf{D}^{(\alpha)} = \eta N_i H_{A,B}^i \left[D^{(\alpha)} \right]^A \left[D^{(\alpha)} \right]^B \tag{23}$$

$$\kappa_n^{(\alpha)} \approx -\eta \mathbf{M}^{(\alpha)} \nabla \mathbf{H} : \mathbf{D}^{(\alpha)} \otimes \mathbf{D}^{(\alpha)} = -\eta M_i H_{A,B}^i \left[D^{(\alpha)} \right]^A \left[D^{(\alpha)} \right]^B \tag{24}$$

$$\tau^{(1)} \approx -\eta \mathbf{N} \nabla \mathbf{H} : \mathbf{D}^{(2)} \otimes \mathbf{D}^{(1)} = -\eta N_i H_{A,B}^i \left[D^{(2)} \right]^A \left[D^{(1)} \right]^B \tag{25}$$

$$\tau^{(2)} \approx -\eta \mathbf{N} \nabla \mathbf{H} : \mathbf{D}^{(1)} \otimes \mathbf{D}^{(2)} = -\eta N_i H_{A,B}^i \left[D^{(1)} \right]^A \left[D^{(2)} \right]^B \tag{26}$$

$$\gamma^{(12)} \approx \eta \mathbf{D}^{(1)} \cdot \mathbf{H} \mathbf{D}^{(2)} + \eta \mathbf{H} \mathbf{D}^{(1)} \cdot \mathbf{D}^{(2)}$$
$$= \eta D_i^{(1)} H_A^i \left[D^{(2)} \right]^A + \eta H_A^i \left[D^{(1)} \right]^A D_i^{(2)} \tag{27}$$

$$\gamma^{(31)} \approx \eta \mathbf{D}^{(3)} \cdot \mathbf{H} \mathbf{D}^{(1)} + \eta \mathbf{H} \mathbf{D}^{(1)} \cdot \mathbf{D}^{(3)}$$
$$= \eta D_i^{(3)} H_A^i \left[D^{(1)} \right]^A + \eta H_A^i \left[D^{(1)} \right]^A D_i^{(3)} \tag{28}$$

$$\gamma^{(32)} \approx \eta \mathbf{D}^{(3)} \cdot \mathbf{H} \mathbf{D}^{(2)} + \eta \mathbf{H} \mathbf{D}^{(3)} \cdot \mathbf{D}^{(2)}$$
$$= \eta D_i^{(3)} H_A^i \left[D^{(2)} \right]^A + \eta H_A^i \left[D^{(3)} \right]^A D_i^{(2)} \tag{29}$$

Consequentially the second order Taylor expansion of the energy density contributions become

$$w_e = \frac{1}{4} K_e \left[\left(u_{,2}^1 + u_{,1}^2 \right)^2 + \left(u_{,1}^1 + u_{,2}^2 \right)^2 \right] \tag{30}$$

$$w_g = \frac{1}{4} K_g \left[4 \left(u_{,21}^3 \right)^2 + \left(u_{,11}^3 + u_{,22}^3 \right)^2 \right] \tag{31}$$

$$w_n = \frac{1}{8} K_n \left[\left(u_{,11}^1 + u_{,22}^1 - 2u_{,12}^2 \right)^2 + \left(u_{,11}^2 + u_{,22}^2 - 2u_{,12}^1 \right)^2 \right] \tag{32}$$

$$w_t = \frac{1}{4} K_t \left[\left(u_{,11}^3 - u_{,22}^3 \right)^2 \right] \tag{33}$$

$$w_{pe} = \frac{1}{2} K_e^{(3)} \left[\left(u_{,3}^3 \right)^2 \right] \tag{34}$$

$$w_s = \frac{1}{2} K_s^{(12)} \left[\left(u_{,1}^1 - u_{,2}^2 \right)^2 \right] \tag{35}$$

$$+ \frac{1}{2} K_s^{(31)} \left[\left(u_{,3}^1 + u_{,3}^2 + u_{,1}^3 + u_{,2}^3 \right)^2 \right] \tag{36}$$

$$+ \frac{1}{2} K_s^{(32)} \left[\left(u_{,3}^1 - u_{,3}^2 + u_{,1}^3 - u_{,2}^3 \right)^2 \right] \tag{37}$$
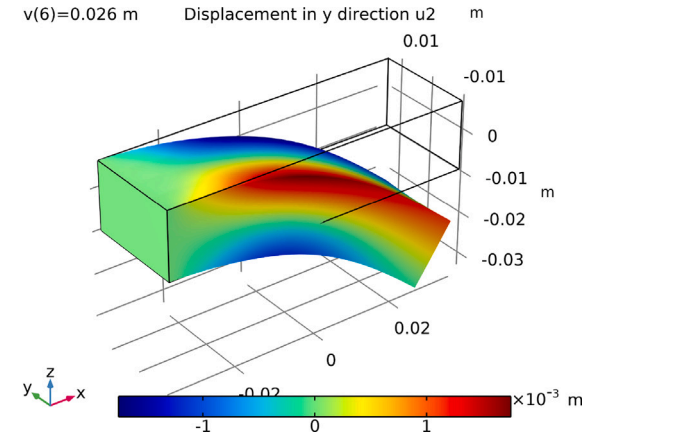
$$w_c = \frac{1}{2} K_c \left[u_{,3}^3 \left(u_{,1}^1 + u_{,2}^2 \right) \right] \tag{38}$$

The sum of these contributions results in the complete internal energy density.

For positive stiffness factors this energy has only infinitesimal rigid body motions as zero-energy modes(floppy modes) given by

$$\mathbf{u}_r = \mathbf{x} \times \boldsymbol{\omega} + \mathbf{b} \tag{39}$$

with constant rotation vector $\boldsymbol{\omega}$ and translation vector $\mathbf{b}$.

Assuming perfect pivots, which correlates with $K_s^{(12)} = 0$, we find an additional floppy mode, with some scalar a, as

$$\mathbf{u}_f = a \left(X^1 \hat{\mathbf{E}}_1 - X^2 \hat{\mathbf{E}}_2 \right) . \tag{40}$$

These floppy modes are similar to discussed ones in [24,25].

Let us note that the form of floppy modes is essential for further studies of well-posedness of the static problem under consideration, see e.g. [24,25]. In particular, for a free pantographic block they result in some constraints for external loadings. More precisely, infinitesimal rigid body motions correspond to the classic self-equilibrium conditions

$$\int_{\Pi} \mathbf{f} \, d\Pi + \int_{\partial \Pi} \mathbf{t} \, dS = \mathbf{0},$$

$$\int_{\Pi} \mathbf{X} \times \mathbf{f} \, d\Pi + \int_{\partial \Pi} \mathbf{X} \times \mathbf{t} \, dS = \mathbf{0},$$

where $\mathbf{f}$ and $\mathbf{t}$ are volume forces and surface traction, respectively. An additional floppy mode (40) gives additional scalar condition

$$\int_{\Pi} \left(X^1 \mathbf{f} \cdot \hat{\mathbf{E}}_1 - X^2 \mathbf{f} \cdot \hat{\mathbf{E}}_2 \right) d\Pi$$

$$+ \int_{\partial \Pi} \left(X^1 \mathbf{t} \cdot \hat{\mathbf{E}}_1 - X^2 \mathbf{t} \cdot \hat{\mathbf{E}}_2 \right) dS = 0.$$

6. Incompleteness

All second derivatives of the displacement only appear due to the curvature terms of the fibers. This means, that there is no coupling in second order between the fiber plane and the third direction along the pivots. Therefore, the energy density is incomplete as not all second order derivatives appear. This can be clearly seen in the linearized model as we get no dependency of w_{int} on $H_{A,B}^i$ for $\{A = 3 \vee B = 3\}$.

7. Simulations

All our simulations use the reference configuration Π as a closed cuboid with $[0, 73]$ mm $\times$ $[0, 24]$ mm $\times$ $[0, 16]$ mm and the fiber orientation from Section 4. We choose stiffness coefficients based on fibers with a rectangular cross-section with Area $A_f = ab$ and pivots with a round cross-section of Area $A_p = \pi r^2$. We call l the distance between pivots in the fiber plane, and h the distance in pivot direction between fiber layers so that $2N = \frac{H}{h}$. With E and J referring to the respective Young's modulus and second moment of area.

$$K_e = \frac{E_f A_f}{lh}, \quad K_n = \frac{E_f J_n}{lh}, \quad K_g = \frac{E_f J_g}{lh}, \quad K_s = 0, \tag{41}$$

$$K_e^{(3)} = \frac{E_p A_p}{l^2}, \quad K_s^{(3)} = (2N - 1) \frac{12 E_p A_p r^2}{2l^2 h^2}, \quad K_c = \nu K_e^{(3)} . \tag{42}$$

Setting $K_s = 0$ is the assumption of a hinge between the beams which is often referred to as perfect pivots. We performed a series of simple showcase simulations including (i) compression and traction test (Fig. 3), (ii) torsion (Fig. 4), (iii) shear (Fig. 5) and (iv) bending (Fig. 5).

8. Conclusion

With this simple energy we can efficiently compute deformation patterns for otherwise complex and computationally expensive beam simulations. As will be shown in following publications, the deformed configurations of experiments are well reflected by our model.

Data availability

No data was used for the research described in the article.

Acknowledgments

References

[1] J.-J. Alibert, P. Seppecher, F. dell'isola, Truss modular beams with deformation energy depending on higher displacement gradients, Math. Mech. Solids 8 (2003) http://dx.doi.org/10.1177/1081286503008001658.

[2] M. Cuomo, F. dell'Isola, L. Greco, Simplified analysis of a generalized bias test for fabrics with two families of inextensible fibres, Z. Angew. Math. Phys. 67 (3) (2016) 61, http://dx.doi.org/10.1007/s00033-016-0653-z.

[3] L. Placidi, E. Barchiesi, E. Turco, N.L. Rizzi, A review on 2D models for the description of pantographic fabrics, Z. Angew. Math. Phys. 67 (5) (2016) 121, http://dx.doi.org/10.1007/s00033-016-0716-1.

[4] F. dell'Isola, P. Seppecher, M. Spagnuolo, E. Barchiesi, F. Hild, T. Lekszycki, I. Giorgio, L. Placidi, U. Andreaus, M. Cuomo, S. Eugster, A. Pfaff, K. Hoschke, R. Langkemper, E. Turco, R. Sarikaya, A. MISRA, M. Angelo, F. D'Annibale, T. Hayat, Advances in pantographic structures: Design, manufacturing, models, experiments and image analyses, Contin. Mech. Thermodyn. 31 (2019) 1231–1282, http://dx.doi.org/10.1007/s00161-019-00806-x.

[5] F. dell'Isola, P. Seppecher, J.J. Alibert, T. Lekszycki, R. Grygoruk, M. Pawlikowski, D. Steigmann, I. Giorgio, U. Andreaus, E. Turco, M. Gołaszewski, N. Rizzi, C. Boutin, V.A. Eremeyev, A. Misra, L. Placidi, E. Barchiesi, L. Greco, M. Cuomo, A. Cazzani, A.D. Corte, A. Battista, D. Scerrato, I.Z. Eremeeva, Y. Rahali, J.-F. Ganghoffer, W. Müller, G. Ganzosch, M. Spagnuolo, A. Pfaff, K. Barcz, K. Hoschke, J. Neggers, F. Hild, Pantographic metamaterials: an example of mathematically driven design and of its technological challenges, Contin. Mech. Thermodyn. 31 (4) (2019) 851–884, http://dx.doi.org/10.1007/s00161-018-0689-8.

[6] A. Ciallella, D.J. Steigmann, Unusual deformation patterns in a second-gradient cylindrical lattice shell: Numerical experiments, Math. Mech. Solids (2022) 10812865221101820, http://dx.doi.org/10.1177/10812865221101820, Publisher: SAGE Publications Ltd STM.

[7] F. dell'Isola, I. Giorgio, M. Pawlikowski, N.L. Rizzi, Large deformations of planar extensible beams and pantographic lattices: heuristic homogenization, experimental and numerical examples of equilibrium, Proc. R. Soc. A 472 (2185) (2016) 20150790, http://dx.doi.org/10.1098/rspa.2015.0790, URL http://rspa.royalsocietypublishing.org/lookup/doi/10.1098/rspa.2015.0790.

[8] H. Abdoul-Anziz, P. Seppecher, Strain gradient and generalized continua obtained by homogenizing frame lattices, Math. Mech. Complex Syst. 6 (3) (2018) 213–250, http://dx.doi.org/10.2140/memocs.2018.6.213, URL https://msp.org/memocs/2018/6-3/p04.xhtml, Publisher: Mathematical Sciences Publishers.

[9] J.F. Ganghoffer, H. Reda, A variational approach of homogenization of heterogeneous materials towards second gradient continua, Mech. Mater. 158 (2021) 103743, http://dx.doi.org/10.1016/j.mechmat.2021.103743, URL https://www.sciencedirect.com/science/article/pii/S0167663621000028.

[10] R. Fedele, Approach à la Piola for the equilibrium problem of bodies with second gradient energies. Part II: Variational derivation of second gradient equations and their transport, Contin. Mech. Thermodyn. (2022) http://dx.doi.org/10.1007/s00161-022-01100-z.

[11] E. Turco, F. dell'Isola, A. Cazzani, N.L. Rizzi, Hencky-type discrete model for pantographic structures: numerical comparison with second gradient continuum models, Z. Angew. Math. Phys. 67 (4) (2016) 85, http://dx.doi.org/10.1007/s00033-016-0681-8.

[12] E. Barchiesi, G. Ganzosch, C. Liebold, L. Placidi, R. Grygoruk, W.H. Müller, Out-of-plane buckling of pantographic fabrics in displacement-controlled shear tests: experimental results and model validation, Contin. Mech. Thermodyn. 31 (1) (2019) 33–45, http://dx.doi.org/10.1007/s00161-018-0626-x.

[13] F. Hild, A. Misra, F. dell'Isola, Multiscale DIC applied to pantographic structures, Exp. Mech. 61 (2) (2021) 431–443, http://dx.doi.org/10.1007/s11340-020-00636-y.

[14] M. Valmalle, A. Vintache, B. Smaniotto, F. Gutmann, M. Spagnuolo, A. Ciallella, F. Hild, Local–global DVC analyses confirm theoretical predictions for deformation and damage onset in torsion of pantographic metamaterial, Mech. Mater. 172 (2022) 104379, http://dx.doi.org/10.1016/j.mechmat.2022.104379, URL https://www.sciencedirect.com/science/article/pii/S0167663622001521.

[15] I. Giorgio, N. Rizzi, U. Andreaus, D. Steigmann, A two-dimensional continuum model of pantographic sheets moving in a 3D space and accounting for the offset and relative rotations of the fibers, Math. Mech. Complex Syst. 7 (2019) 311–325, http://dx.doi.org/10.2140/memocs.2019.7.311.

[16] I. Giorgio, V. Varano, F. dell'Isola, N.L. Rizzi, Two layers pantographs: A 2D continuum model accounting for the beams' offset and relative rotations as averages in SO(3) Lie groups, Int. J. Solids Struct. 216 (2021) 43–58, http://dx.doi.org/10.1016/j.ijsolstr.2021.01.018, URL https://www.sciencedirect.com/science/article/pii/S0020768321000263.

[17] A. Ciallella, D. Pasquali, F. D'Annibale, I. Giorgio, Shear rupture mechanism and dissipation phenomena in bias-extension test of pantographic sheets: Numerical modeling and experiments, Math. Mech. Solids (2022) 10812865221103573, http://dx.doi.org/10.1177/10812865221103573, Publisher: SAGE Publications Ltd STM.

[18] M.E. Yildizdag, E. Barchiesi, F. dell'Isola, Three-point bending test of pantographic blocks: numerical and experimental investigation, Math. Mech. Solids 25 (10) (2020) 1965–1978, http://dx.doi.org/10.1177/1081286520916911, Publisher: SAGE Publications Ltd STM.

[19] I. Giorgio, N.L. Rizzi, E. Turco, Continuum modelling of pantographic sheets for out-of-plane bifurcation and vibrational analysis, Proc. R. Soc. A 473 (2207) (2017) 20170636, http://dx.doi.org/10.1098/rspa.2017.0636, URL https://royalsocietypublishing.org/doi/full/10.1098/rspa.2017.0636.

[20] R. Fedele, A. Ciani, L. Galantucci, M. Bettuzzi, L. Andena, A regularized, pyramidal multi-grid approach to global 3D-volume digital image correlation based on X-ray micro-tomography, Fund. Inform. 125 (3–4) (2013) 361–376.

[21] S.R. Eugster, Numerical analysis of nonlinear wave propagation in a pantographic sheet, Math. Mech. Complex Syst. 9 (3) (2022) 293–310.

[22] A. Battista, L. Rosa, R. dell'Erba, L. Greco, Numerical investigation of a particle system compared with first and second gradient continua: Deformation and fracture phenomena*, Math. Mech. Solids 22 (11) (2017) 2120–2134, http://dx.doi.org/10.1177/1081286516657889, Publisher: SAGE Publications Ltd STM.

[23] M. Spagnuolo, M.E. Yildizdag, X. Pinelli, A. Cazzani, F. Hild, Out-of-plane deformation reduction via inelastic hinges in fibrous metamaterials and simplified damage approach, Math. Mech. Solids 27 (6) (2022) 1011–1031, http://dx.doi.org/10.1177/10812865211052670, Publisher: SAGE Publications Ltd STM.

[24] V.A. Eremeyev, F. dell'Isola, C. Boutin, D. Steigmann, Linear pantographic sheets: Existence and uniqueness of weak solutions, J. Elasticity 132 (2) (2018) 175–196, http://dx.doi.org/10.1007/s10659-017-9660-3.

[25] V.A. Eremeyev, F.S. Alzahrani, A. Cazzani, F. dell'Isola, T. Hayat, E. Turco, V. Konopińska-Zmysłowska, On existence and uniqueness of weak solutions for linear pantographic beam lattices models, Contin. Mech. Thermodyn. 31 (6) (2019) 1843–1861, http://dx.doi.org/10.1007/s00161-019-00826-7.